Time shifts in photoemission from a fully correlated two-electron model system

S. Nagele,[1,*] R. Pazourek,[1,†] J. Feist,[2] and J. Burgdörfer[1]

[1]*Institute for Theoretical Physics, Vienna University of Technology, 1040 Vienna, Austria, EU*

[2]*ITAMP, Harvard-Smithsonian Center for Astrophysics, Cambridge, Massachusetts 02138, USA*

(Received 19 December 2011; published 1 March 2012)

We theoretically investigate time-resolved photoemission originating from two different shells ($1s$ and $2p$) of a fully correlated atomic two-electron model system ionized by an extreme-ultraviolet attosecond light pulse. The parameters of the model system are tuned such that the ionization potentials of the $1s$ and $2p$ electrons have values close to those of the $2s$ and $2p$ levels in a neon atom, for which a relative time delay has been measured in a recent attosecond streaking experiment by Schultze *et al.* [Science **328**, 1658 (2010)]. Up to now theoretical efforts could account only for delays more than a factor of 2 shorter than the reported experimental value. By solving the time-dependent Schrödinger equation numerically *exactly* we explore the influence of correlations on the time delay previously implicated as one of the potential sources of discrepancies. We investigate the influence of the interplay between electron interactions and the probing streaking infrared field on the extracted relative delays between the two emission channels. We find that for our model system the inclusion of electronic correlation only slightly modifies the time shifts, as compared to a mean-field treatment. In particular, the correlation-induced time delay is contained in the Eisenbud-Wigner-Smith time delay for the photoionization process.

DOI: 10.1103/PhysRevA.85.033401 PACS number(s): 32.80.Fb, 42.50.Hz, 42.65.Re, 31.15.A−

I. INTRODUCTION

Attosecond streaking is one of the most fundamental processes in attosecond science [1–7], and an attosecond streak camera [8] allows for an accurate characterization of isolated attosecond extreme-ultraviolet (XUV) pulses, as well as the *clocking of ultrafast electronic dynamics* in atoms, molecules, and solids. The basic idea of attosecond streaking is that electrons which are emitted in the presence of an infrared (IR) laser field are accelerated to different final momenta, depending on their release time. Thus, temporal information is mapped to the energy domain. Pioneering experiments include the direct measurement of light waves [9], temporal measurements of the decay time of Auger processes in krypton [10], and transport of electrons in tungsten surfaces [11].

In a recent paper, the measurement of a time delay of 21 ± 5 as between the photoemission of neon $2s$ or $2p$ electrons was reported by Schultze *et al.* [1]. This work triggered considerable interest [12–19] since a significant fraction of the observed delay could not be explained by state-of-the-art quantum-mechanical calculations [1]. Meanwhile, delays in photoionization have also been measured for the emission of argon $3s$ and $3p$ electrons using a complementary, interferometric technique [20].

Schultze *et al.* employed several theoretical approaches to account for the observed time shifts in Ne: the time-dependent Schrödinger equation (TDSE) in the single-active-electron (SAE) approximation using a model potential for Ne yielded group delays of the XUV wave packets corresponding to ionization from the $2s$ and $2p$ shell (without an IR field) of 4.5 as after spectral averaging. A similar value was obtained by simulating the streaking experiment, including both the IR and the XUV pulses, using the Coulomb-Volkov approximation (CVA) and extracting the time shifts from the resulting streaking spectrograms (cf. [15]). Use of the TDSE instead of the CVA gave a slightly higher time shift of 6.8 as. Many-electron models which partially include the effect of electron correlation on the time shifts were employed to analyze the dipole transition matrix elements for photoionization by the XUV pulse. The multiconfigurational Hartree-Fock method (MCHF) yielded a time shift of 4.0 as. The state-specific expansion approach (SSEA) [21], which better accounts for electronic correlation by including interchannel couplings, gave a slightly larger delay of 6.4 as. Subsequently Kheifets and Ivanov [12] analyzed the dipole matrix elements using the (independent-electron) Hartree-Fock (HF) approximation and found a time shift of 6.2 as. An improved calculation using the random-phase approximation with exchange (RPAE) gave 8.4 as.

All theoretical approaches up to now fail to *quantitatively* account for the observed experimental delay. Very recently Ivanov and Smirnova [19] suggested that the discrepancies between experiment and theory could be resolved by doubling the theoretical delays obtained in [12] (and hence also in [1]) to account for modifications of the time shifts by the streaking field. We show in this paper that such a procedure is not valid for the present one- and two-active-electron models.

A complete and conclusive theoretical *ab initio* treatment of the XUV photoionization process in the presence of the streaking field would require a converged numerical solution of the TDSE for a neon atom exposed to the attosecond XUV pulse and the IR streaking field. Clearly, the complexity of the corresponding ten-electron wave function precludes a fully correlated time-dependent treatment without severe approximations.

In this contribution we will focus on a model two-electron system for which the TDSE can be solved numerically exactly with the help of supercomputers. The model potentials $V_{N-2}(r_i)$, representing the interaction with the core consisting of the nucleus and $N-2$ electrons, are chosen such that the lowest two states of opposite parity, in the following referred

*stefan.nagele@tuwien.ac.at

†renate.pazourek@tuwien.ac.at

to as $1s$ and $2p$, have binding energies close to those of the neon $2s$ and $2p$ subshells. The corresponding nonrelativistic Hamilton operator of such a system reads in atomic units

$$H_0 = \frac{\vec{p}_1^{\,2}}{2} + V_{N-2}(r_1) + \frac{\vec{p}_2^{\,2}}{2} + V_{N-2}(r_2) + \frac{1}{|\vec{r}_1 - \vec{r}_2|}, \quad (1)$$

where $\vec{r}_i$ and $\vec{p}_i$ are the canonical coordinates of the ith electron which is subject to the radial-symmetric potential $V_{N-2}(r_i)$ representing the mean field generated by the remaining $N-2$ electrons ($N=10$ for neon). The mutual electronic repulsion is mediated by the two-body Coulomb interaction operator $\frac{1}{|\vec{r}_1-\vec{r}_2|}$. We refer to this model Hamiltonian as the two-active-electron (TAE) approximation.

Unlike the authors of previous works [1,12], we do not aim for an accurate description of the electronic structure of neon. Rather, we want to investigate whether electronic correlation, if treated exactly in a fully *ab initio* fashion, gives rise to time delays substantially different from those found in a mean-field treatment. Furthermore, simulating a prototypical streaking experiment allows us to determine whether the interplay between correlations and the IR field noticeably affects the observable relative time shifts. Atomic units will be used throughout the text unless indicated otherwise.

II. SINGLE-ACTIVE-ELECTRON APPROACH FOR NEON

We first briefly review the SAE, or mean-field, treatment of the time delay in photoemission as observed in an attosecond streaking setup. To simulate the interaction of the ionizing XUV pulse and the IR streaking field with an atom (e.g., neon) in the SAE approximation, we solve the three-dimensional TDSE

$$i\frac{\partial}{\partial t}\Psi(\vec{r},t) = \left[-\frac{\vec{\nabla}^2}{2} + V_{N-1}(r) + \vec{r}\cdot[\vec{F}_{\rm XUV}(t) + \vec{F}_{\rm IR}(t)]\right]\Psi(\vec{r},t), \quad (2)$$

where $\vec{F}_{\rm XUV}(t)$ is the (linearly polarized) electric field of the attosecond pump pulse, $\vec{F}_{\rm IR}(t)$ is the (linearly polarized) electric field of the few-cycle IR probe pulse, and $V_{N-1}(r)$ is a model potential obtained from self-interaction-free density-functional theory [22] representing the mean field generated by the remaining $N-1$ electrons. The electric fields are related to the corresponding vector potentials by $\vec{F}(t) = -\frac{\partial}{\partial t}\vec{A}(t)$. The computational method is based on the well-established pseudospectral split-operator technique as described in [23]. The temporal propagation is carried out using a split-operator algorithm where the evolution under the influence of the field-free Hamiltonian is performed in the energy representation of the wave function and the evolution driven by the external field is calculated in the length gauge on a grid in coordinate space.

Extraction of time shifts by streaking originally was inspired by the strong-field approximation (SFA), which establishes a simple, approximate relation between the unperturbed asymptotic momentum of the photoelectron $\vec{p}_0$ and the final momentum $\vec{p}_f(\tau)$ for emission at time τ in the presence of an IR field,

$$\vec{p}_f(\tau) = \vec{p}_0 - \vec{A}_{\rm IR}(\tau). \quad (3)$$

After independently simulating the streaking protocol for the $2s$ and $2p_0$ initial states, we thus extract the absolute time shifts by fitting the first moments of the final momentum distribution $\vec{p}_f(\tau)$ to the modified momentum $\vec{p}_0 - \alpha\vec{A}_{\rm IR}(t+t_{\rm S})$, where α is a correction factor for the amplitude of the momentum shift induced by the streaking field, and the sign convention for $t_{\rm S}$ ensures that positive (negative) values correspond to delayed (advanced) emission relative to the center of the XUV pulse. The $2p_1$ and $2p_{-1}$ initial states can be neglected since they do not contribute significantly to the photoelectron emission in the direction of the laser polarization axis.

We investigated the absolute time shifts $t_{\rm S}$ for different XUV energies in the range from 40 to 140 eV which are plotted in Fig. 1 as a function of the final electron energy. For an XUV energy of 106 eV (as in the neon experiment), we obtain a relative streaking delay of $\Delta t_{\rm S} = t_{\rm S}^{2p} - t_{\rm S}^{2s} \approx 6.9$ as between emission from $2s$ and $2p$. This agrees well with the TDSE value of 6.8 as reported in [1], which was obtained from another model potential for Ne and with a different numerical algorithm. However, as has been shown recently [13,14,19], the simultaneous interaction of the outgoing electron with the streaking IR field and the Coulomb potential ("Coulomb-laser coupling" cf. [24,25]) leads to an apparent streaking time (or phase) shift that does not originate from the timing of the XUV ionization process but can be explained classically from the combined influence of the streaking and Coulomb fields on the outgoing electron trajectory [13], or by use of the eikonal approximation [14]. This goes clearly beyond the SFA, which by construction does not include any Coulomb-laser coupling (CLC) effects. The magnitude of the apparent continuum CLC time shift $t_{\rm CLC}$ for neon can be accurately extracted from the Coulombic hydrogen $1s$ streaking delays $t_{\rm S}^{\rm H}$ for the same field parameters. This procedure is justified since exit-channel CLC for continuum electrons emitted from neon has its origin in the long-ranged, asymptotic $1/r$, *hydrogenic* Coulomb potential.

However, the streaking time shifts $t_{\rm S}^{\rm H}$, which are in very good approximation equivalent to the delays obtained from corresponding classical simulations [13], do not stem from Coulomb-laser coupling alone but also contain information on the spectral phase, i.e., the group delay or Eisenbud-Wigner-Smith (EWS) delay $t_{\rm EWS}$ [26–28], of the XUV wave packet [29]. Thus, we split the total streaking time shifts into two contributions,

$$t_{\rm S} \approx t_{\rm EWS} + t_{\rm CLC}, \quad (4)$$

where $t_{\rm EWS}$ for a pure Coulomb potential has its origin in the energy dependence of the Coulomb phase $\sigma_\ell = \arg\Gamma(\ell+1-iZ/\sqrt{2E})$ which depends on the angular momentum ℓ and with $Z=1$ for a singly ionized atom. For the present case the Coulomb correction thus yields

$$t_{\rm CLC} \approx t_{\rm S}^{\rm H} - \frac{d}{dE}\sigma_1. \quad (5)$$

The correction term $t_{\rm CLC}$ (red solid line in Fig. 1) decreases with increasing energy of the outgoing electron E

approximately as $\sim -E^{-3/2}$ [13,30]. The EWS time delays $t_{\rm EWS}$ can be related to the dipole transition matrix elements between the initial state ψ_i and final state ψ_f,

$$t_{\rm EWS} = \frac{d}{dE} \arg[\langle \psi_f(E,\theta=0)|\hat{z}|\psi_i\rangle], \tag{6}$$

which are evaluated in forward direction $\theta = 0^\circ$ (as are the streaking spectrograms). For the simplest case of an initial s state resulting in a pure p continuum, the expression in Eq. (6) reduces to the (partial-wave) time delay $\frac{d}{dE}(\delta_1 + \sigma_1)$, where δ_ℓ is the elastic-scattering phase shift due to the short-ranged contributions (which fall off faster than r^{-1}) to the radial potential $V_{N-1}(r)$. Note that the additional centrifugal contribution to the EWS delay due to the energy dependence of σ_ℓ is specific to Coulomb potentials. The corresponding (regular) asymptotic continuum partial-wave solutions for $Z = 1$ are proportional to $\sin\left(kr + \frac{\ln 2kr}{k} - \frac{\ell\pi}{2} + \sigma_\ell + \delta_\ell\right)$ with $k = \sqrt{2E}$. For an initial p state both the s and d continua in Eq. (6) add up coherently.

The relative CLC correction for the present final electron energies for ionization of Ne $2s$ and $2p$ states by a 106 eV XUV pulse in the SAE approximation gives $\Delta t_{\rm CLC} \approx 2.8$ as. The remaining relative delay of $\Delta t_{\rm S} - \Delta t_{\rm CLC} \approx 4.1$ as follows from the differences in the spectral phases of the $2s$ and $2p$ wave packets, i.e., the relative EWS time delay.

If we add the EWS time delays $t_{\rm EWS}$, independently determined from the dipole matrix element in Eq. (6), to the CLC delays $t_{\rm CLC}$ (red solid line in Fig. 1), the resulting curves for $t_{\rm EWS} + t_{\rm CLC}$ as functions of the final electron energy (green and blue dashed lines) coincide with the simulated streaking shifts $t_{\rm S}$ (open squares and circles, respectively). This near perfect agreement demonstrates that, on the one-electron level, streaking time shifts can be well accounted for by adding up the EWS-like shifts and the independent CLC contributions, $t_{\rm S} \approx t_{\rm EWS} + t_{\rm CLC}$. Consequently, no additional measurement-induced time shifts due to the combined effect of the laser field and the short-ranged parts of the potential $V_{N-1}(r)$ are observed. In particular, doubling the value of the short-ranged EWS delays, as suggested in [19], would destroy the very good agreement between $t_{\rm S}$ and $t_{\rm CLC} + t_{\rm EWS}$.

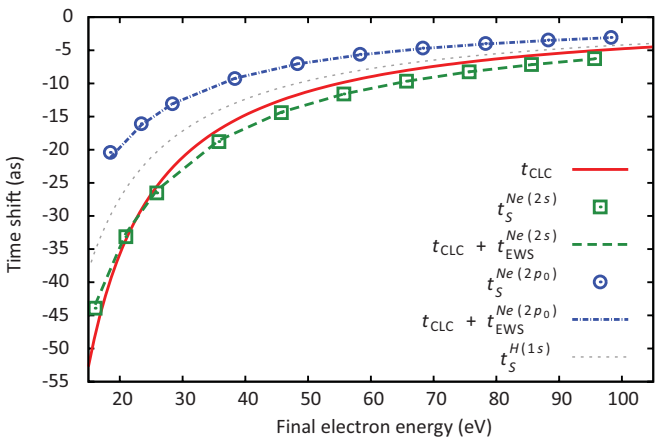

FIG. 1. (Color online) Streaking time shifts $t_{\rm S}$ extracted from quantum-mechanical simulations for $2s$ (green squares) and $2p_0$ (blue circles) initial states of a Ne one-electron model potential (see text). The results are obtained from spectrograms taken in the forward direction with respect to the laser polarization axis. Using an opening angle of 10° instead has almost no influence on the obtained delays. The dashed green (and blue) lines show the results of adding the corresponding Eisenbud-Wigner-Smith time delays $t_{\rm EWS}$ for $2s$ (and $2p_0$) to the Coulomb-laser coupling time shifts $t_{\rm CLC}$ (red solid line) which almost perfectly equal the streaking delays (squares and circles). The streaking results for H($1s$) (gray dotted line) are shown for comparison.

The physical origin of the different EWS time shifts lies in the short-ranged contributions of the model potential $V_{N-1}(r)$, which approximately account for the many-electron effects in the SAE treatment, and in the differences in the centrifugal potential that the outgoing electrons encounter; cf. [29]. One extension is worth noting: polarization of the initial state [16,29] by the streaking field can, in principle, give additional contributions to Eq. (4) (cf. [12]). In the present case, the initial state has a small polarizability and entrance channel distortions can be safely ignored. This was verified by performing constrained TDSE calculations ("restricted ionization model" [31,32]) in which the initial-state interaction with the IR field is suppressed but continuum states fully evolve under the influence of the IR field. As expected, the obtained streaking delays (not shown) are in excellent agreement with the full TDSE results shown in Fig. 1.

Since the short-ranged part of the model potential $V_{N-1}(r)$, reflects, on the mean-field level, many-electron effects, $t_{\rm EWS}$ approximates the time delay caused by the mean field. The question to what extent the approximation holds for a true two-electron (or more generally, many-electron) process will be addressed below.

III. TWO-ACTIVE-ELECTRON APPROXIMATION

The parameters of our two-electron model system are chosen such that, to some degree, it mimics a neon atom: as an initial state we use the fully correlated $1s2p\ ^1P^{\rm o}$ eigenfunction of our model Hamiltonian [Eq. (1)], so that the initial state of the emitted electron will have either s or p angular momentum character. With this choice the photoemission will occur from two energetically well-separated levels accessing the same partial-wave sectors as for neon. We tailor the model potential such that the ionization potentials of the s and p electrons take approximately the same values as for the $2s$ and $2p$ levels in Ne. In addition, the $1s2p$ initial state has to be sufficiently isolated in energy so that the IR field cannot noticeably couple to neighboring states of the model system, which would lead to unwanted modifications of the streaking process. Along the same lines, the initial state and the remaining ionic states should have a low polarizability in order to avoid entrance- or exit-channel distortions. One simple (but, clearly, not unique) realization of these constraints is provided by the model potential

$$V_{N-2}(r) = -\frac{\tilde{Z}}{r} + V_0 e^{-(r-r_0)^2/d^2}, \tag{7}$$

consisting of a pure Coulomb potential with a superimposed, short-ranged Gaussian contribution. The choice of $\tilde{Z} = 2$ ensures that in the case of single ionization the outgoing electron is asymptotically exposed to a long-ranged Coulombic tail which decays as $1/r$. The short-ranged potential mimics

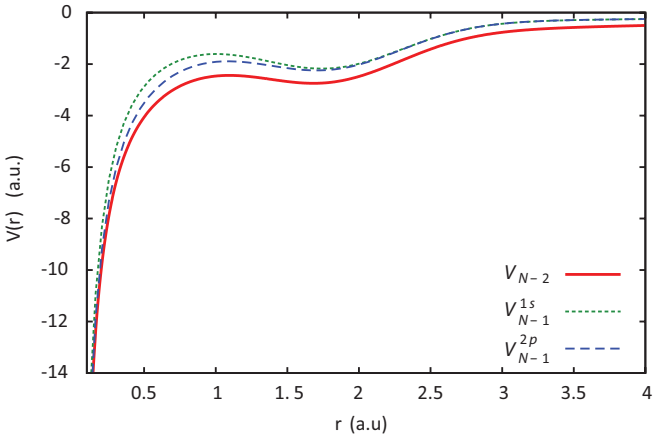

FIG. 2. (Color online) Radial potential $V_{N-2}(r)$ [Eq. (7)] for the two-active-electron model (red solid line), and reduced mean-field potentials $V^{2p}_{N-1}(r)$ (blue dashed line) and $V^{1s}_{N-1}(r)$ (green dotted line), derived from the charge distributions of a $1s$ or $2p$ electron, entering the SAE analysis.

the mean field of the remaining $N-2$ electrons ($N \geqslant 3$) of a many-electron atom. In our simulations we use the parameter set $V_0 = -1.6$ a.u., $r_0 = 1.8$ a.u., and $d = 0.72$ a.u. (Fig. 2). This choice results in an ionization potential of the TAE system of $I_{2p} = 23.1$ eV for the $2p$ electron (as compared to 21.6 eV for neon) and $I_{1s} = 49.8$ eV for the $1s$ electron (as compared to 48.5 eV for $2s$ of neon). The residual shift in the ionization potentials of about 1.5 eV for both states can be easily compensated for by slightly increasing the XUV energy to achieve the same final electron energies as in the experiment.

In our computational approach (see, e.g., [33,34] for a detailed description) we numerically solve the TDSE for the TAE system. To that end we expand the six-dimensional wave function $\Psi(\vec{r}_1,\vec{r}_2)$ in coupled spherical harmonics $\mathcal{Y}^{LM}_{l_1,l_2}(\Omega_1,\Omega_2)$,

$$\Psi(\vec{r}_1,\vec{r}_2,t) = \sum_{L,M}^{\infty}\sum_{l_1,l_2}^{\infty} \frac{R^{LM}_{l_1,l_2}(r_1,r_2,t)}{r_1 r_2}\mathcal{Y}^{LM}_{l_1,l_2}(\Omega_1,\Omega_2), \qquad (8)$$

which results in a set of coupled partial differential equations in r_1 and r_2 ("time-dependent close-coupling" [35–37]). The radial degrees of freedom are treated using a finite-element discrete-variable representation (FEDVR) [38–40], which leads to block-diagonal kinetic matrices and allows for an efficient parallelization. We employ an explicit temporal propagation using the short-iterative Lanczos (SIL) algorithm [41,42] with automatic time stepping and error control. The $1s2p$ initial state is obtained by solving the stationary Schrödinger equation, i.e., by directly diagonalizing the full two-electron Hamiltonian, using the Arnoldi package (ARPACK) [43] which implements the implicitly restarted Arnoldi method.

Since we study only single ionization where one electron remains bound to the nucleus, we use an asymmetric (L-shaped) radial grid where only one of the two radial coordinates becomes "asymptotically" large. The same idea can be exploited in the angular partial-wave expansion since only the continuum electron, subject to the IR-field-induced quiver motion, will reach high angular momenta. Note that exchange symmetry remains fully preserved when this asymmetric decomposition of coordinate space is applied. In order to keep the outgoing electron in the computational box, we use a radial grid extending to 816 a.u., whereas the radial coordinate of the second electron is restricted to 96 a.u., large enough to accommodate the excited ionic states up to $n = 8$. Doubly ionized parts of the wave function are absorbed by a complex absorbing potential at the box boundaries. Each FEDVR element spans a length of 4.0 a.u. and contains a DVR of order 11. The partial-wave expansion covers total angular momenta up to $L = 8$ and one-electron angular momenta up to $l_< = 5$ for the inner and $l_> = 8$ for the outer electron. The external fields are linearly polarized and treated in dipole approximation. Thus, we can restrict ourselves to partial waves with total magnetic quantum number $M = 0$ due to the cylindrical symmetry of the system. Our simulations are checked for convergence with respect to the size of the angular and radial bases.

IV. RESULTS AND DISCUSSION

In Fig. 3 we show the resulting streaking spectrograms for photoionization of the $1s2p$ neonlike initial state taken in the forward direction with respect to the laser polarization axis. The XUV pulse has a central photon energy of 107.5 eV and a duration of 200 as (FWHM of the Gaussian intensity envelope). The XUV intensity was chosen to be 10^{13} W/cm^2 which is, presumably, higher than in the experiment but still well in the perturbative, one-photon regime. The 800 nm IR streaking field has a duration of 3 fs (FWHM of the $\cos^2$ envelope) and an intensity of 4×10^{11} W/cm^2. As has been shown previously [13], the intensity of the streaking IR field does not noticeably affect the streaking time shifts. In addition,

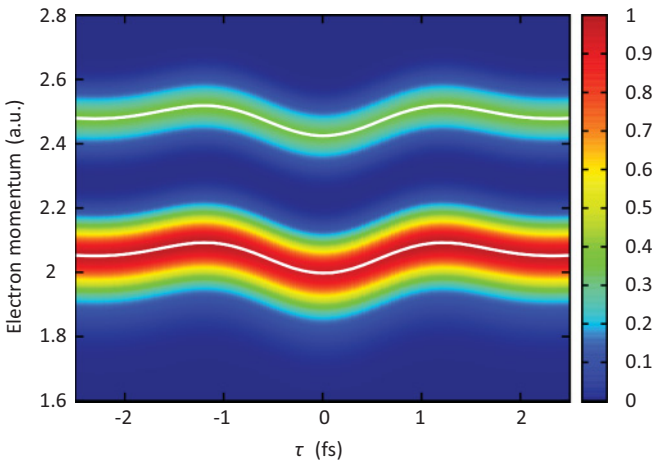

FIG. 3. (Color online) Streaking spectrogram for a $1s2p$ initial state of the model system ionized by an XUV pulse with a photon energy of 107.5 eV and duration of 200 as [full width at half maximum (FWHM) of the Gaussian intensity envelope]. The figure shows the final momentum distribution in the forward direction with respect to the laser polarization axis as a function of the delay time τ between the IR and the XUV pulses. The streaking field has a wavelength of 800 nm, a duration of 3 fs, and an intensity of 4×10^{11} W/cm^2. The solid white lines are the first moments of the electron spectra.

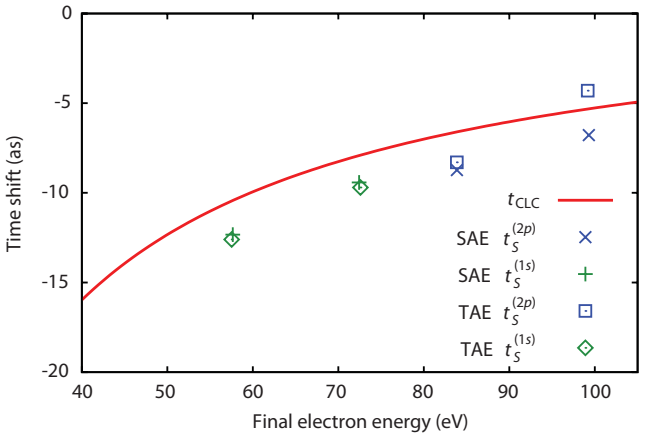

FIG. 4. (Color online) Streaking time shifts t_S extracted from quantum-mechanical two-electron simulations for the fully correlated model system [Eq. (1)] subject to XUV pulses with energies of 107.5 and 122.4 eV for an emitted $2p$ electron, $(1s,Es)$ and $(1s,Ed)$ final channels (blue squares), and a $1s$ electron, $(2p,Ep)$ final channel (green diamonds). The crosses show the corresponding SAE calculations where one of the two electrons was kept frozen (see text). The SAE as well as the TAE results are obtained from spectrograms taken in the forward direction with respect to the laser polarization axis. Use of an opening angle of 10° instead has almost no influence on the obtained delays. For comparison we also show the Coulomb-laser coupling time shifts t_{CLC} (red solid line).

we verified their insensitivity to the XUV peak intensity in the range between 10^{12} and 10^{15} W/cm^2.

By fitting the first moment of the two emission channels in the momentum spectrograms Fig. 3 to the analytic form of the IR vector potential, we obtain a relative time shift of $\Delta t_S \approx 4.3$ as (see Fig. 4). As in the Ne experiment the emission of the asymptotically faster p electron appears to be delayed with respect to the slower s electron. However, quantitatively, the extracted delay is still well below the experimental value and on the same level as the previously reported theoretical results for Ne. For the present final energies of 83.9 and 57.5 eV, the expected offset due to the hydrogenic CLC is about $\Delta t_{CLC} \approx 3.5$ as (see the red line in Fig. 4). The remaining relative time shift of only $\Delta t_S - \Delta t_{CLC} \approx 0.8$ as agrees well with the relative EWS time delay of $\Delta t_{EWS} \approx 0.9$ as obtained from the group delay of the XUV wave packet (evaluated in the forward direction and averaged over the wave packet's spectral width). Note that the accuracy of this decomposition [Eq. (4)] also persists on the level of absolute time shifts (see Table I). Schultze *et al.* have carried out another set of streaking measurements with XUV pulses of higher energy and longer duration [1]. In analogy, we also repeated the TAE simulations for a second XUV pulse with a photon energy of 122 eV and a duration of 400 as (FWHM), very close to the experimental parameters. While for the lower photon energy the relative time shifts are dominated by the CLC term, for the higher photon energy the EWS time delay becomes more important (see Table I). The decomposition into the contributions from CLC and the EWS delay [Eq. (4)] holds for both energies.

It is now instructive to perform a reduced SAE analysis for the same model system for which the TAE description

TABLE I. Absolute streaking time shifts t_S, Coulomb-laser coupling corrections t_{CLC}, and Eisenbud-Wigner-Smith delays t_{EWS} for the two-active-electron simulations and the corresponding reduced mean-field single-active-electron analysis for two different XUV pulses. The sum $t_{CLC} + t_{EWS}$ agrees very well with the streaking delays t_S according to Eq. (4). All numbers are given in attoseconds.

	t_{CLC}	t_{EWS}	$t_{CLC} + t_{EWS}$	t_S
107 eV XUV pulse				
TAE model $(1s)$	−9.5	−3.2	−12.7	−12.6
SAE model $(1s)$	−9.5	−2.8	−12.3	−12.3
TAE model $(2p)$	−6.0	−2.3	−8.3	−8.3
SAE model $(2p)$	−6.0	−2.9	−8.9	−8.7
122 eV XUV pulse				
TAE model $(1s)$	−7.2	−2.6	−9.8	−9.7
SAE model $(1s)$	−7.2	−2.3	−9.5	−9.4
TAE model $(2p)$	−4.8	0.8	−4.0	−4.3
SAE model $(2p)$	−4.8	−2.0	−6.8	−6.8

is possible. To this end we construct the corresponding mean-field potentials $V_{N-1}^{1s}(r)$ and $V_{N-1}^{2p}(r)$ from the fully correlated $1s2p$ wave function $\Psi_{1s2p}(\vec{r}_1,\vec{r}_2)$. We can exploit the fact that the corresponding partial-wave expansion (8) is largely dominated (>99% of the initial norm) by the two terms $R^{L=1M=0}_{l_1=0,l_2=1}(r_1,r_2) = R^{L=1M=0}_{l_1=1,l_2=0}(r_2,r_1)$. Tracing out one coordinate then gives the screening charge distributions of the frozen $1s$ electron,

$$|\Phi^{1s}(r_1)|^2 = 2\int \left|\frac{R^{L=1M=0}_{l_1=0,l_2=1}(r_1,r_2)}{r_1 r_2}\right|^2 r_2^2 dr_2 \left|Y_0^0(\Omega_1)\right|^2, \quad (9)$$

which is radially symmetric, and the angle-dependent charge distributions of the frozen $2p$ electron

$$|\Phi^{2p}(\vec{r}_2)|^2 = 2\int \left|\frac{R^{L=1M=0}_{l_1=0,l_2=1}(r_1,r_2)}{r_1 r_2}\right|^2 r_1^2 dr_1 \left|Y_0^1(\Omega_2)\right|^2, \quad (10)$$

where $Y_m^\ell(\Omega)$ are the spherical harmonics. In the present case, the resulting orbitals are essentially equivalent to singly occupied natural orbitals constructed from a decomposition of $\Psi_{1s2p}(\vec{r}_1,\vec{r}_2)$ [44]. The mean-field Hartree potentials can then be obtained from

$$V_{N-1}^{1s,2p}(\vec{r}) = V_{N-2}(r) + \int d^3\vec{r}\,' \frac{|\Phi^{1s,2p}(\vec{r}\,')|^2}{|\vec{r}-\vec{r}\,'|}. \quad (11)$$

In the present case, the resulting anisotropy for the $V_{N-1}^{2p}(\vec{r})$ potential is small and can be neglected, which facilitates the computational treatment. This procedure results in mean-field ionization potentials $I_{2p} = 24.2$ eV for the $2p$ and $I_{1s} = 51.9$ eV for the $1s$ electron, which are very close to the values obtained from the full two-electron initial state. Repeating the streaking simulation with the same field parameters as in the TAE case (but with slightly higher XUV energies to compensate for the differences in the ionization potentials), we find a relative time delay $\Delta t_S \approx 3.6$ as for the lower photon energy. Subtraction of the CLC delay according to Eq. (4) gives

very good agreement with the corresponding relative EWS time delay extracted from the one-electron mean-field dipole matrix elements Eq. (6). As for the TAE case, Eq. (4) also holds true on the sub-1-as level for the absolute time shifts (Table I). For the lower photon energy, comparison with the two-active-electron calculation (see Fig. 4 or Table I) shows that there are no significant time shifts due to two-electron correlation effects beyond the effective mean-field level. For the more energetic and longer XUV pulse, the discrepancy between the SAE and the fully correlated TAE results is somewhat larger. This pertains mainly to the highly energetic $2p$ electron, the EWS time shift of which is more strongly influenced by electronic correlations that cannot be incorporated by a simple (Hartree) mean-field treatment. Note that this discrepancy already exists on the level of the EWS time shifts and is not affected by the streaking field (see Table I). Thus, in the SAE as well as in the TAE approximation, Eq. (4) is fulfilled on the sub-1-as level for the absolute and relative time shifts. In particular, the remarkably good agreement of the streaking delays with the CLC-corrected EWS delays shows that the interplay between electron-electron interactions and the IR field does not affect the observable time shifts. This also holds true for the case where correlation has a noticeable effect on the EWS delay.

In conclusion, we have evaluated streaking time shifts on the independent-electron level using a single-active-electron or mean-field model potential for Ne as well as for a fully correlated two-active-electron model system mimicking, to some extent, a neon atom. The streaking time delays from the SAE simulations using a Ne model potential agree well with results of previous studies, which are considerably lower than the experimental value. We show that in all cases the time delay is given by the sum of the EWS and CLC contributions Eq. (4). Thus, the Eisenbud-Wigner-Smith delay, which stems from the XUV transition matrix elements alone, can be obtained from the streaking spectrograms, if the apparent time shifts from Coulomb-laser coupling in the exit channel are accounted for.

The two-electron model allows one to study the photoemission of two interacting correlated electrons from two distinct shells with energy levels similar to those in the Ne atom, even though the mean-field potential representing the remaining electrons does not accurately represent the electronic structure of neon. Also, in the TAE model simulations with pulse parameters as in the experiment, we found very good agreement between the CLC-corrected EWS delays and the streaking time shifts. We can thus infer that the laser field does not strongly affect the electronic interaction and the related time shifts, during photoemission. Comparison with SAE calculations, where one electron is kept frozen, demonstrates that this holds true even when correlation becomes important in the photoemission process, i.e., when the EWS delays from the SAE and TAE models differ. We found that also in a time-dependent, fully correlated treatment electronic intershell interaction *per se* does not induce large enough time shifts to match the experimental value. In the present case, relative time shifts are dominated by the one-electron exit-channel Coulomb-laser coupling contributions. This latter observation may, however, be specific to the present model system, which focuses on intershell correlations. Furthermore, no additional measurement-induced time shifts due to the interaction of the probing IR streaking field with the short-ranged parts of the model potentials could be identified. The explanation of the experimentally observed time delay between photoemission of the $2p$ and $2s$ states in neon remains an open problem.

Note added. Very recently we became aware of the publication of work by Moore *et al.* [45], who performed many-electron time-dependent studies using the R-matrix incorporating time method. They simulated a streaking setup for the ionization of neon by a 105.2 eV XUV pulse and obtained a time delay of 10.2 ± 1.3 as between emission from the $2s$ and $2p$ orbitals.

ACKNOWLEDGMENTS

This work was supported by the FWF-Austria, Grants No. SFB016 and No. P21141-N16, and in part by the National Science Foundation through TeraGrid resources provided by NICS and TACC under Grant No. TG-PHY090031. The computational results presented have also been achieved in part using the Vienna Scientific Cluster (VSC). R.P. acknowledges support by the TU Vienna Doctoral Program "Functional Matter" and J.F. by the NSF through a grant to ITAMP.

[1] M. Schultze, M. Fiess, N. Karpowicz, J. Gagnon, M. Korbman, M. Hofstetter, S. Neppl, A. L. Cavalieri, Y. Komninos, T. Mercouris, C. A. Nicolaides, R. Pazourek, S. Nagele, J. Feist, J. Burgdörfer, A. M. Azzeer, R. Ernstorfer, R. Kienberger, U. Kleineberg, E. Goulielmakis, F. Krausz, and V. S. Yakovlev, Science **328**, 1658 (2010).

[2] M. Hentschel, R. Kienberger, C. Spielmann, G. A. Reider, N. Milosevic, T. Brabec, P. Corkum, U. Heinzmann, M. Drescher, and F. Krausz, Nature (London) **414**, 509 (2001).

[3] M. Drescher, M. Hentschel, R. Kienberger, G. Tempea, C. Spielmann, G. A. Reider, P. B. Corkum, and F. Krausz, Science **291**, 1923 (2001).

[4] R. Kienberger, E. Goulielmakis, M. Uiberacker, A. Baltuska, V. Yakovlev, F. Bammer, A. Scrinzi, T. Westerwalbesloh, U. Kleineberg, U. Heinzmann, M. Drescher, and F. Krausz, Nature (London) **427**, 817 (2004).

[5] V. S. Yakovlev, F. Bammer, and A. Scrinzi, J. Mod. Opt. **52**, 395 (2005).

[6] F. Quéré, Y. Mairesse, and J. Itatani, J. Mod. Opt. **52**, 339 (2005).

[7] G. Sansone, E. Benedetti, F. Calegari, C. Vozzi, L. Avaldi, R. Flammini, L. Poletto, P. Villoresi, C. Altucci, R. Velotta, S. Stagira, S. De Silvestri, and M. Nisoli, Science **314**, 443 (2006).

[8] J. Itatani, F. Quéré, G. L. Yudin, M. Y. Ivanov, F. Krausz, and P. B. Corkum, Phys. Rev. Lett. **88**, 173903 (2002).

[9] E. Goulielmakis, M. Uiberacker, R. Kienberger, A. Baltuska, V. Yakovlev, A. Scrinzi, T. Westerwalbesloh, U. Kleineberg, U. Heinzmann, M. Drescher, and F. Krausz, Science **305**, 1267 (2004).

[10] M. Drescher, M. Hentschel, R. Kienberger, M. Uiberacker, V. Yakovlev, A. Scrinzi, T. Westerwalbesloh, U. Kleineberg, U. Heinzmann, and F. Krausz, Nature (London) **419**, 803 (2002).
[11] A. L. Cavalieri, N. Müller, T. Uphues, V. S. Yakovlev, A. Baltuška, B. Horvath, B. Schmidt, L. Blümel, R. Holzwarth, S. Hendel, M. Drescher, U. Kleineberg, P. M. Echenique, R. Kienberger, F. Krausz, and U. Heinzmann, Nature (London) **449**, 1029 (2007).
[12] A. S. Kheifets and I. A. Ivanov, Phys. Rev. Lett. **105**, 233002 (2010).
[13] S. Nagele, R. Pazourek, J. Feist, K. Doblhoff-Dier, C. Lemell, K. Tőkési, and J. Burgdörfer, J. Phys. B **44**, 081001 (2011).
[14] C. H. Zhang and U. Thumm, Phys. Rev. A **82**, 043405 (2010).
[15] V. S. Yakovlev, J. Gagnon, N. Karpowicz, and F. Krausz, Phys. Rev. Lett. **105**, 073001 (2010).
[16] J. C. Baggesen and L. B. Madsen, Phys. Rev. Lett. **104**, 043602 (2010).
[17] C. H. Zhang and U. Thumm, Phys. Rev. A **84**, 033401 (2011).
[18] A. S. Kheifets, I. A. Ivanov, and I. Bray, J. Phys. B **44**, 101003 (2011).
[19] M. Ivanov and O. Smirnova, Phys. Rev. Lett. **107**, 213605 (2011).
[20] K. Klünder, J. M. Dahlström, M. Gisselbrecht, T. Fordell, M. Swoboda, D. Guénot, P. Johnsson, J. Caillat, J. Mauritsson, A. Maquet, R. Taïeb, and A. L'Huillier, Phys. Rev. Lett. **106**, 143002 (2011).
[21] C. A. Nicolaides, T. Mercouris, and Y. Komninos, J. Phys. B **35**, L271 (2002).
[22] X. M. Tong and C. D. Lin, J. Phys. B **38**, 2593 (2005).
[23] X. M. Tong and S. I. Chu, Chem. Phys. **217**, 119 (1997).
[24] O. Smirnova, M. Spanner, and M. Y. Ivanov, J. Phys. B **39**, S323 (2006).
[25] O. Smirnova, A. S. Mouritzen, S. Patchkovskii, and M. Y. Ivanov, J. Phys. B **40**, F197 (2007).
[26] L. Eisenbud, Ph.D. thesis, Princeton University, 1948.
[27] E. P. Wigner, Phys. Rev. **98**, 145 (1955).
[28] F. T. Smith, Phys. Rev. **118**, 349 (1960).
[29] R. Pazourek, S. Nagele, K. Doblhoff-Dier, J. Feist, C. Lemell, K. Tőkési, and J. Burgdörfer, e-print arXiv:1111.4172.
[30] C. W. Clark, Am. J. Phys. **47**, 683 (1979).
[31] K. J. Schafer, in *Strong Field Laser Physics*, Springer Series in Optical Sciences, Vol. 134, edited by T. Brabec (Springer, New York, 2009) Chap. 6, pp. 111–145.
[32] J. Mauritsson, P. Johnsson, E. Mansten, M. Swoboda, T. Ruchon, A. L'Huillier, and K. J. Schafer, Phys. Rev. Lett. **100**, 073003 (2008).
[33] J. Feist, S. Nagele, R. Pazourek, E. Persson, B. I. Schneider, L. A. Collins, and J. Burgdörfer, Phys. Rev. A **77**, 043420 (2008).
[34] B. I. Schneider, J. Feist, S. Nagele, R. Pazourek, S. X. Hu, L. A. Collins, and J. Burgdörfer, in *Quantum Dynamic Imaging*, CRM Series in Mathematical Physics, edited by A. D. Bandrauk and M. Ivanov (Springer, Berlin, 2011), Chap. 10.
[35] J. Colgan and M. S. Pindzola, Phys. Rev. Lett. **88**, 173002 (2002).
[36] S. Laulan and H. Bachau, Phys. Rev. A **68**, 013409 (2003).
[37] M. S. Pindzola, F. Robicheaux, S. D. Loch, J. C. Berengut, T. Topcu, J. Colgan, M. Foster, D. C. Griffin, C. P. Ballance, D. R. Schultz, T. Minami, N. R. Badnell, M. C. Witthoeft, D. R. Plante, D. M. Mitnik, J. A. Ludlow, and U. Kleiman, J. Phys. B **40**, R39 (2007).
[38] T. N. Rescigno and C. W. McCurdy, Phys. Rev. A **62**, 032706 (2000).
[39] C. W. McCurdy, D. A. Horner, and T. N. Rescigno, Phys. Rev. A **63**, 022711 (2001).
[40] B. I. Schneider and L. A. Collins, J. Non-Cryst. Solids **351**, 1551 (2005).
[41] T. J. Park and J. C. Light, J. Chem. Phys. **85**, 5870 (1986).
[42] E. S. Smyth, J. S. Parker, and K. T. Taylor, Comput. Phys. Commun. **114**, 1 (1998).
[43] K. Maschhoff and D. C. Sorensen, Appl. Parallel Comput. Ind. Comput. Optim. **1184**, 478 (1996).
[44] P. O. Löwdin and H. Shull, Phys. Rev. **101**, 1730 (1956).
[45] L. R. Moore, M. A. Lysaght, J. S. Parker, H. W. van der Hart, and K. T. Taylor, Phys. Rev. A **84**, 061404 (2011).